Bioorganic Chemistry 90 (2019) 103076

Contents lists available at ScienceDirect

Bioorganic Chemistry

journal homepage: www.elsevier.com/locate/bioorg

Dihydrofolate reductase inhibition effect of 5-substituted pyrido[2,3-*d*] pyrimidines: Synthesis, antitumor activity and molecular modeling study

Ola A. Abdelaziz, Walaa M. El Husseiny, Khalid B. Selim*, Hassan M. Eisa

Department of Pharmaceutical Organic Chemistry, Faculty of Pharmacy, Mansoura University, Mansoura 35516, Egypt

ARTICLE INFO

Keywords:
Pyrido[2,3-*d*]pyrimidine
DHFR inhibitor
Antitumor activity
Apoptosis
Cell cycle arrest

ABSTRACT

A new series of pyrido[2,3-*d*]pyrimidines **3–18** bearing substitution at C-5 position was synthesized. All compounds were tested for their *in vitro* antitumor activity against five human cancer cell lines namely; hepatocellular carcinoma (HePG2), breast carcinoma (MCF-7), human prostate carcinoma (PC3), colorectal carcinoma (HCT-116), and cervical carcinoma (Hela) using doxorubicin as a positive control. Compounds **3**, **4**, **9**, **11**, **13**, **14**, **15** and **17** exhibited the highest antitumor activity against the tested cell lines and were selected to screen their enzymatic inhibition against dihydrofolate reductase enzyme (DHFR) compared with the reference drug methotrexate (MTX), to explain the probable mechanism of action of the observed anticancer activity. Compound **11** displayed the highest inhibitory activity (IC_{50} = 6.5 μM) among the tested compounds in comparison with MTX (IC_{50} = 5.57 μM). Also, compounds **13** and **14** showed high inhibitory activity against DHFR with IC_{50} values 7.1 and 8.7 μM, respectively. Comparative molecular modeling study was performed between DHFR inhibitors **11**, **13** and **14** of the highest activity and **10** of the lowest activity among the eight inhibitors against MTX. Docking studies into the active site of DHFR domain showed good agreement with the obtained biological results. Finally, compound **11** was found to be best antitumor, DHFR inhibitor, and it induced the process of apoptosis at Pre-G phase and cell cycle arrest at G2/M phase in MCF-7 cells.

1. Introduction

Dihydrofolate reductase (DHFR) catalyzes the reduction of dihydrofolate (DHF) to tetrahydrofolate (THF) using nicotinamide adenine dinucleotide phosphate (NADPH) as cofactor·THF is essential for *de novo* synthesis of purine and thymidylate (TMP) in cell proliferation [1]. Inhibition of DHFR activity results in cell death [2], so that DHFR becomes an important target enzyme in the development of chemotherapy [3]. Antifolates are classified into classical type such as methotrexate (MTX) and non-classical type such as piritrexim (PTX) and trimetrexate (TMQ) [4]. In classical type, the hydrophilic nature of the inhibitor, due to its glutamate moiety, limits its transport into the cells by diffusion so, an active transport mechanism is essential. However, in non-classical type, replacing of the hydrophilic glutamate moiety by lipophilic groups leads to enhancement of its transport into the cells by passive diffusion [5,6] (Fig. 1).

Many derivatives of pyrido[2,3-*d*]pyrimidine are very potent inhibitors of DHFR [7] and play an important role in DNA intercalation because of their structural resemblance to a purine- pyrimidine complementary base pair [8]. Analysis of the structure of these DHFR inhibitors declares that pyrido[2,3-*d*]pyrimidine ring of PTX can form hydrogen bonds with DHFR in which the binding mode is similar to the analogous ring of MTX [9]. 2,4-Diamino substitution of pyrido[2,3-*d*] pyrimidine is critical for inhibitory activity because the 2-amino group can form an important hydrogen bond with Glu30 and the 4-amino group can form other hydrogen bonds with Ile7 and Val115 [10]. Protonation of N-1 enables the formation of an electrostatic interaction with Glu30 [11], in addition, the presence of 5-methyl group highly increases the inhibition potency by forming hydrophobic bond with Val115 [11]. Methylene amine (CH_2-NH) linker exhibits better activity than methylene (CH_2) linker in PTX [12,13]. Moreover, nitrogen atom at position 10 was found to be important for activity [14]. Phenyl ring at C-6 linked through CH_2-NH is essential for DHFR inhibitory activity, especially when it is carrying polar substituents (e.g. Cl and OCH_3), also the positions of the substituents on phenyl ring had a significant effect on the potency [15,16]. Derivatives having 2,5-dimethoxy phenyl which are regarded as structural novel analogs of PTX showed similar binding mode into the DHFR active site as PTX binding [4] (Fig. 2).

This work was targeted to design novel candidates of antitumor drugs, which are structurally related to MTX having lipophilic side chain instead. The synthesized compounds were assessed for their *in vitro* cytotoxicity against a panel of five tumor cell lines, namely,

* Corresponding author.
E-mail address: khbselim@mans.edu.eg (K.B. Selim).

https://doi.org/10.1016/j.bioorg.2019.103076
Received 22 March 2019; Received in revised form 7 June 2019; Accepted 17 June 2019
Available online 18 June 2019
0045-2068/

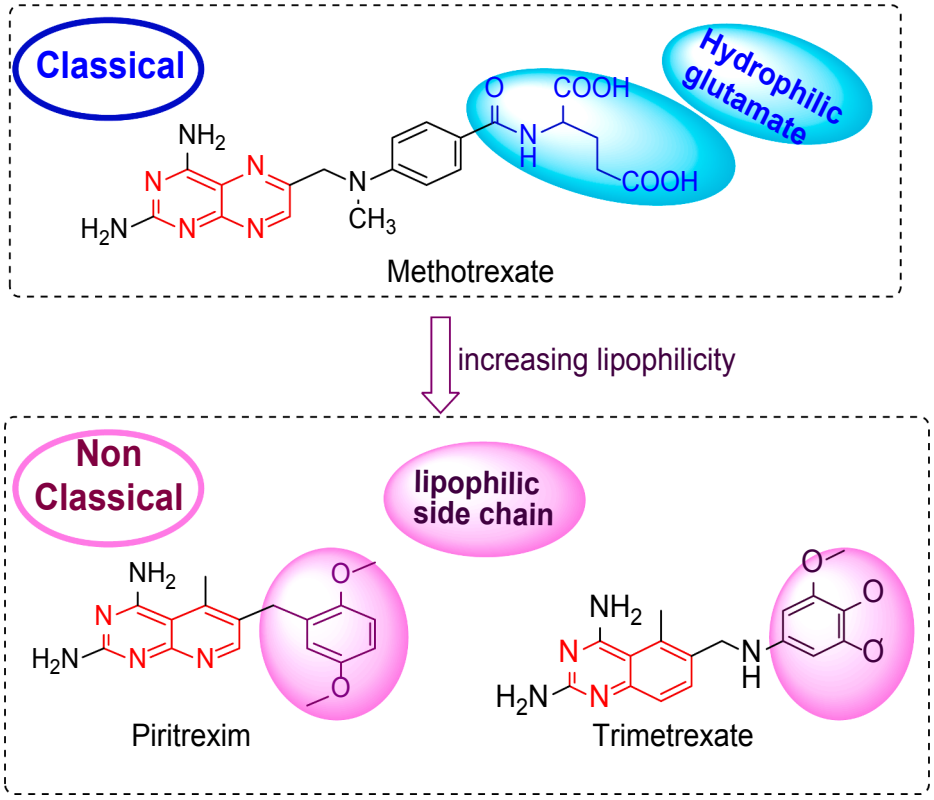

Fig. 1. Structural classification of antifolate drugs.

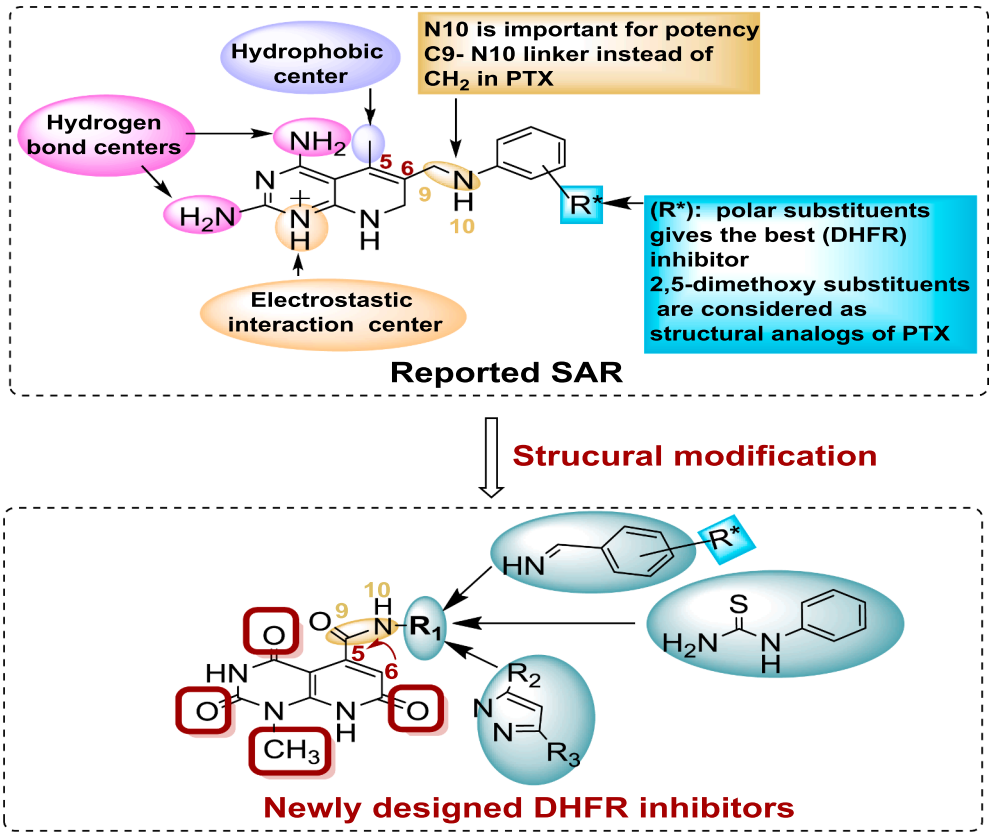

Fig. 2. Reported SAR of pyrido[2,3-*d*]pyrimidine derivatives and the newly designed DHFR inhibitors.

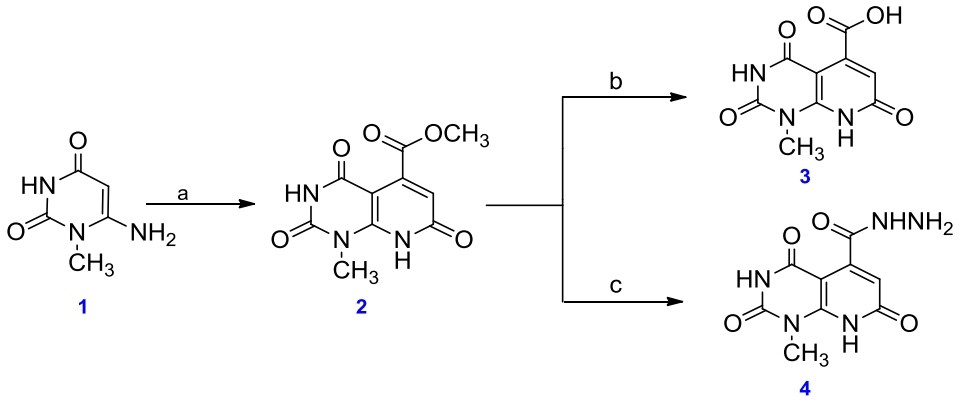

Scheme 1. Reagents and reaction conditions: (a) DMAD, H_2O, 100 °C, (b) NaOH, MeOH, 85 °C and (c) $NH_2NH_2{\cdot}7H_2O$, EtOH, 90 °C.

hepatocellular carcinoma (HePG2), breast carcinoma (MCF-7), human prostate carcinoma (PC3), colorectal carcinoma (HCT-116), and cervical carcinoma (Hela). Furthermore, the most potent compounds were tested for their effect on cell death and cell cycle distribution in addition to the enzymatic inhibitory potency on DHFR (as a probable believable mechanism of their antitumor efficacy).

2. Results and discussion

2.1. Chemistry

The synthesis of the target compounds is shown in Schemes 1 and 2. Pyrido[2,3-*d*]pyrimidine-5-carboxylate **2** was prepared by the reaction of pyrimidine-2,4(1*H*,3*H*)-dione **1** with dimethyl acetylenedicarboxylate (DMAD) in aqueous medium [17] (Scheme 1). The carboxylate compound **2** was hydrolyzed in basic conditions (NaOH/MeOH) to give pyrido[2,3-*d*]pyrimidine-5-carboxylic acid **3** [18]. The structure of the carboxylic acid **3** was confirmed by ^{1}H NMR spectrum through the disappearance of OCH_3 protons of the ester at 3.71 ppm and the appearance of highly deshielded acidic proton at 12.4 ppm. Moreover, it was confirmed by IR spectroscopy *via* the disappearance of (CO) of the ester band at 1740 cm^{-1} and the appearance of (CO) of acid band at 1700 cm^{-1}, beside, the appearance of broad band of (OH) at 3455 cm^{-1}.

The key intermediate pyrido[2,3-*d*]pyrimidine-5-carbohydrazide **4** was prepared in a good yield through refluxing methyl carboxylate ester **2** with hydrazine hydrate in ethanol [19]. The structure of hydrazide **4** was confirmed using IR spectroscopy by the disappearance of (CO) of ester band at 1740 cm^{-1} and the appearance of (CO) of hydrazide band at 1680 cm^{-1}. Also, the characteristic peaks of (NH_2) and (NH) were appeared at 3349, 3282 and 3143 cm^{-1}, respectively. Besides, ^{1}H NMR spectrum showed the appearance of NH proton at 9.05 ppm and NH_2 protons at 11.13 ppm along with the disappearance of signal of OCH_3 protons 3.71 ppm.

As shown in Scheme 2, the target hydrazones **5–13** were prepared by the condensation of hydrazide **4** with several aromatic aldehydes in

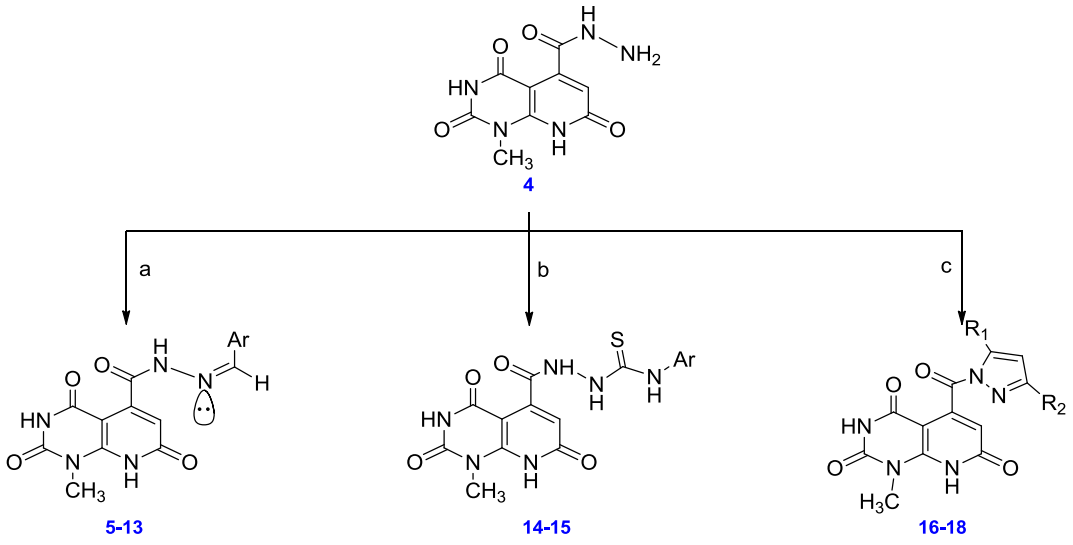

5: Ar = 3-NO_2-Ph
6: Ar = 4-NO_2-Ph
7: Ar = 4-F-Ph
8: Ar = 4-HO-Ph
9: Ar = 4-Me_2N-Ph
10: Ar = 4-F-2-MeO-Ph
11: Ar = 3-HO-4-MeO-Ph
12: Ar = 3,4-diMeO-Ph
13: Ar = 2,5-diMeO-Ph

14: Ar = Ph
15: Ar = 4-NO_2-Ph

16: R_1, R_2 = CH_3
17: R_1 = CH_3, R_2 = OC_2H_5
18: R_1 = CH_3, R_2 = Ph

Scheme 2. Reagents and reaction conditions: (a) appropriate aromatic aldehydes, EtOH, 90 °C, (b) appropriate 1,3-dicarbonyl compounds, EtOH, 90 °C, (c) appropriate aromatic isothiocyanate, DMF, r.t.

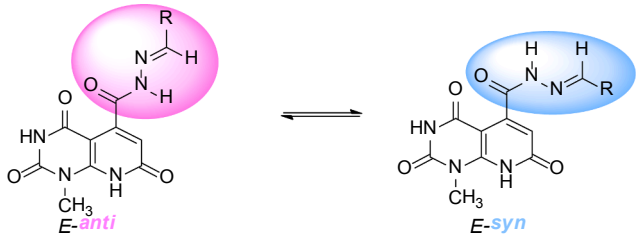

Fig. 3. Stereochemistry and general structure of NAH.

absolute ethanol [20]. ^{1}H NMR of **5–13** showed the signal of ylidenic proton (HC═N) of all compounds at the range of 7.81–8.46 ppm. Moreover, IR spectroscopy showed characteristic bands at 1560–1578 cm^{-1} attributed to the presence of (C═N) [21,22].

N-acylhydrazones (NAH) **5–13** showed duplication of proton signals in their ^{1}H NMR spectra. *Palla* and coworkers [23] stated that NAH compounds derived from the condensation of hydrazides and aromatic aldehydes are present in solution as the *E* geometric isomer, which is less sterically hindered compared to the *Z* form. The *Z* isomer can be detected in less polar solvents due to its stabilization with intramolecular H-bonds [24]. Therefore, the duplication of NMR signals can be due to C═N double bond stereoisomers (*E/Z*) or CO-NH bond conformers (*syn* and *anti*). Studies showed that aryl-NAH existed in form of two CO-NH bond-related conformations [25]. ^{1}H NMR spectroscopy in polar solvent such as dimethyl sulphoxide (DMSO) showed the *E*-stereoisomerism of hydrazones **5–13** but as a mixture of *syn* and *anti*-conformers.

In the current work, two sets of *E-syn and E-anti* isomers showed ratios ranging from 1:1 to 1.8:1 (Fig. 3). Ylidenic proton (CH═N) showed nearly the same chemical shift value at the range of 7.9–8.0 ppm in all hydrazones.

The reaction of hydrazide **4** with aryl isothiocyanate derivatives in DMF at room temperature [26,27] afforded carbothioamide derivatives **14** and **15**. The structures were confirmed *via* ^{1}H NMR by the appearance of the aromatic protons at the range of 7.17–8.35 ppm and the newly formed NH protons at 10.6 and 11.9 ppm**.** Moreover, they were confirmed in the IR spectrum by the appearance of (C═S) absorption band at 1287 cm^{-1} [28–30] (Scheme 2).

The pyrazole derivatives **16–18** were prepared through Knorr pyrazole reaction between hydrazide **4** and 1,3-dicarbonyl compounds in absolute ethanol [31,32]. The structures of these derivatives were confirmed *via* ^{1}H NMR by the appearance of CH-Pyrazole proton at the range of 6.5–7.5 ppm and CH_3 protons as singlet peak at the range of 1.8–2.0 ppm. Moreover, they were confirmed in IR spectrum by the disappearance of absorption bands of (CO), (NH_2) and (NH) of hydrazide **4** at 1680, 3349, 3282 and 3143 cm^{-1}, respectively (Scheme 2).

2.2. Biology

2.2.1. In vitro cytotoxicity screening

The cytotoxic activities of the novel synthesized compounds **3–18** were evaluated against five tumor cell lines including hepatocellular carcinoma (HePG2), breast carcinoma (MCF-7), human prostate carcinoma (PC3), colorectal carcinoma (HCT-116), and cervical carcinoma (Hela) in comparison to doxorubicin (DOX) as a positive control and the results are summarized in Table 1. Compound **6** with substituent at the *para* position showed higher activity than compound **5** with substituent at the *meta* position [15]. It is clear that compounds **5**, **6** and **7** with electron withdrawing groups (NO_2 and F) exhibited low antitumor activity. Introduction of one electron donating group in compound **8** increased antitumor activity. Compounds **9**, **11** and **13** with two electron donating groups (OH and OMe) showed potent antitumor activity. Compound **11** having polar substituent showed the highest Activity [16]. Compound **13** having 2,5-dimethoxy phenyl moiety was structurally analogs of potent PTX [4]. Compound **14** and **15** were also highly cytotoxic as they are thiourea derivatives which were identified to have important role in DHFR inhibition [33].

2.2.2. In vitro cytotoxicity against human normal cells

To explore whether the newly synthesized compounds exhibited selective cytotoxicity between normal and cancer cells, the most active compound **11** was evaluated against two human normal cell lines including MCF10A (breast) and THLE-2 (liver). Compounds **11** exhibited lower toxicity towards MCF10A cells (IC_{50} = 62.65 μM) and THLE2 cells (IC_{50} = 83.43 μM) in comparison to DOX (IC_{50} = 10.34 and 15.79 μM) against MCF10A and THLE-2, respectively. Compound **11** had a lower toxic effect than DOX on the normal MCF10A and THLE2 cells (Table 2).

2.2.3. Human DHFR enzyme inhibition assay

Compounds **3**, **4**, **9**, **11**, **13**, **14**, **15** and **17** which displayed the highest activity against the five tumor cell lines, were selected for human DHFR inhibition assay relative to MTX as a reference drug. Compound **11** displayed the highest inhibitory activity (IC_{50} = 6.5 μM) among the tested compounds in comparison with MTX (IC_{50} = 5.57 μM). Moreover, compounds **13** and **14** showed high inhibitory activity against DHFR with IC_{50} values 7.1 and 8.7 μM, respectively (Table 3). Compounds **3**, **4**, **9**, **15** and **17** showed good inhibitory activity against DHFR with IC_{50} values 11, 10.7, 9.1, 9.3 and 10 μM, respectively. The cytotoxicity of the selected compounds against MCF-7 (as representative cell line) exhibited an excellent matching with the enzymatic inhibition of DHFR parallel with the calculating docking interaction energy values. These results strongly suggested that the DHFR inhibitory mechanism might be one of the main modes of action of the antitumor activity of the tested compounds.

2.2.4. Molecular modeling

2.2.4.1. Molecular docking study. Computational molecular docking study was achieved to clear up the interaction between the tested compounds and DHFR by using MOE. The docking study was carried out on inhibitors **3**, **11**, **13** and **14** as the ligands, where the structure of complex of DHFR and MTX was selected as the docking model (PDB code 1U72), (Fig. 4) [34–37].

Hydrogen binding pattern of MTX with the DHFR receptor active site showed the formation of three stable H-bonds with the key pocket residue Glu30, and trifurcated H-bonds with the 'catalytic triad' residues of hDHFR pocket Ile7, Tyr121 and Val115. Furthermore, H-bonds are formed with Asn64 [38] (Fig. 4).

Molecular modeling study was essentially needed to understand and interpret the DHFR inhibitory pattern of this new class of pyrido[2,3-*d*] pyrimidines. It was interesting to start a comparative modeling study between DHFR inhibitors **11**, **13** and **14** of the highest activity and **3** of the lowest activity among the eight inhibitors in comparison to MTX. The tertiary complex of human dihydrofolate reductase (hDHFR), NADPH and MTX were used as references for modeling and docking. In general, compounds **11**, **13** and **14** interact with Glu30 through pyridine moiety, they also bind with Asn64 through amide linker moiety in **11**, **13** and of pyrimidine moiety in **14** (Fig. 5).

For compounds **11** and **13,** binding poses show that their scaffolds are buried deeply inside the pocket, with a tortuous "L" structure through the bridge region. They can bind through their pyrimidine moiety to key pocket residue Val115. Compounds **11** and **13** have similar structures but have different enzymatic activity, each compound has its unique pattern of binding, where the most active compound **11** can bind through its pyrimidine moiety to key pocket residue Arg70 which is regarded as another conserved feature of DHFR [7]. Phe31, which is not one of the key residues in the recognition of the parent ligand MTX, plays an essential role in the binding of compound **11** through its hydroxyl group**.** This binding explains the reduced activity of **13** where the hydroxyl group is removed. This finding showed the

Table 1
In vitro cytotoxic activities (IC_{50}, μM) of the synthesized compounds 3–18.

Compound	*In vitro* cytotoxicity IC_{50} (μM)				
	HePG-2	MCF-7	PC3	HCT-116	Hela
3	13.46 ± 1.9	7.22 ± 1.4	10.88 ± 1.8	19.55 ± 0.1.3	8.55 ± 1.1
4	13.52 ± 1.8	7.76 ± 0.7	11.49 ± 1.4	13.47 ± 1.9	40.63 ± 1.3
5	42.86 ± 4.1	36.32 ± 3.8	46.80 ± 4.8	47.60 ± 5.1	> 100
6	30.32 ± 3.5	25.27 ± 3.2	33.53 ± 3.6	40.45 ± 3.9	36.06 ± 4.0
7	26.87 ± 3.0	30.54 ± 3.5	36.14 ± 3.9	28.6 ± 3.6	41.54 ± 4.4
8	21.04 ± 2.4	15.06 ± 1.6	20.91 ± 1.9	22.03 ± 2.7	23.62 ± 3.5
9	**5.93 ± 0.9**	**7.51 ± 1.2**	**16.72 ± 2.3**	**8.28 ± 1.2**	**12.58 ± 1.9**
10	19.15 ± 2.7	16.80 ± 2.3	24.05 ± 3.2	23.18 ± 3.0	27.79 ± 3.8
11	**6.14 ± 0.6**	**5.66 ± 0.4**	**9.21 ± 1.1**	**7.12 ± 0.8**	**6.24 ± 0.9**
12	37.47 ± 3.8	19.13 ± 2.7	26.26 ± 3.5	36.62 ± 4.6	45.53 ± 4.7
13	**6.34 ± 1.3**	**6.49 ± 1.9**	22.28 ± 2.8	**10.56 ± 1.5**	**9.17 ± 2.7**
14	**6.60 ± 0.9**	**6.99 ± 0.7**	**9.01 ± 1.1**	**10.56 ± 0.8**	**9.32 ± 0.7**
15	**12.55 ± 1.7**	**9.88 ± 1.5**	**10.55 ± 1.6**	**8.92 ± 1.1**	**8.93 ± 1.0**
16	33.56 ± 3.5	24.66 ± 3.1	19.44 ± 2.8	12.88 ± 3.0	11.90 ± 2.7
17	**11.55 ± 1.8**	13.55 ± 1.5	**9.55 ± 1.0**	35.77 ± 3.8	**7.88 ± 0.9**
18	29.78 ± 2.5	17.44 ± 2.3	28.66 ± 2.1	12.55 ± 3.0	30.33 ± 3.08
DOX	4.50 ± 0.2	4.17 ± 0.2	8.87 ± 0.6	5.23 ± 0.3	5.57 ± 0.4

Table 2
Cytotoxic activity (IC_{50}) of the most active compound 11 against human normal cells.

Compound	*In vitro* cytotoxicity IC_{50} (μM)	
	MCF10 A	THLE-2
11	62.65 ± 4.42	83.43 ± 6.21
DOX	10.34 ± 3.78	15.79 ± 5.51

Table 3
IC_{50} values of compounds **3**, **4**, **9**, **11**, **13**, **14**, **15** and **17** against DHFR and docking interaction energy.

Compound	Enzymatic IC_{50} (μM)	Docking interaction energy (kcal/ mol)	*In vitro* cytotoxicity IC_{50} (μM) MCF-7
3	11.1	−10.5	7.22 ± 1.4
4	10.7	−10	7.76 ± 0.7
9	9.1	−12.1	7.51 ± 1.2
11	6.5	−14.2	5.66 ± 0.4
13	7.1	−14	6.49 ± 1.9
14	8.7	−13	6.99 ± 0.7
15	9.3	−11.8	9.88 ± 1.5
17	10	−11	13.55 ± 1.5
MTX	5.57	−14.7	–

necessity of such polar hydroxyl group for maximum activity (Fig. 5a and b). For compound **14**, it did not bind to Val115 which seemed to be important for human DHFR binding site [39] (Fig. 5c). This explains the slight difference in enzymatic inhibition activity between **14** and both **11** and **13**.

For compound **3,** it can bind with Val115 only through pyrimidine moiety. However, it did not bind to the key amino acid Glu30 and it was found to be positioned in a linear arrangement. These findings explain its reduced activity among the DHFR inhibitors in comparison with compounds **11**, **13** and **14** (Fig. 5d).

2.2.4.2. Ligand alignment technique. Ligand-based pocket site alignment is a widely adopted technique for the structural analysis of protein–ligand complexes [40]. Good alignment between compounds **11** and MTX explains its activity as shown in Fig. 6a. Fig. 6b indicates different alignment profiles for compounds **13** and MTX, while, Fig. 6c showed that compound **14** is positioned in a linear arrangement.

2.2.5. Cell cycle arrest analysis

The cytotoxic effect of the antitumor drugs might be because of induction of apoptosis and/or cell cycle arrest [41]. To explore that, MCF-7 cells were treated with compound **11** for 24 h, stained with propidium iodide and DNA contents were measured by flow cytometry (Table 4 and Fig. 7). Compared with the control, compound **11** decreased cell proportions at S phase to 19.86% in comparison to the control cells (26.97%). In addition, it increased the cell proportion at

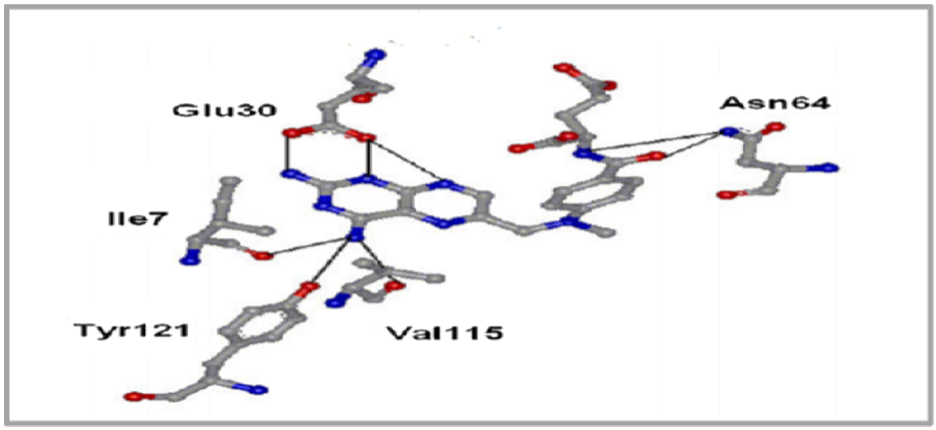

Fig. 4. 2D binding mode and residues involved in the recognition of MTX.

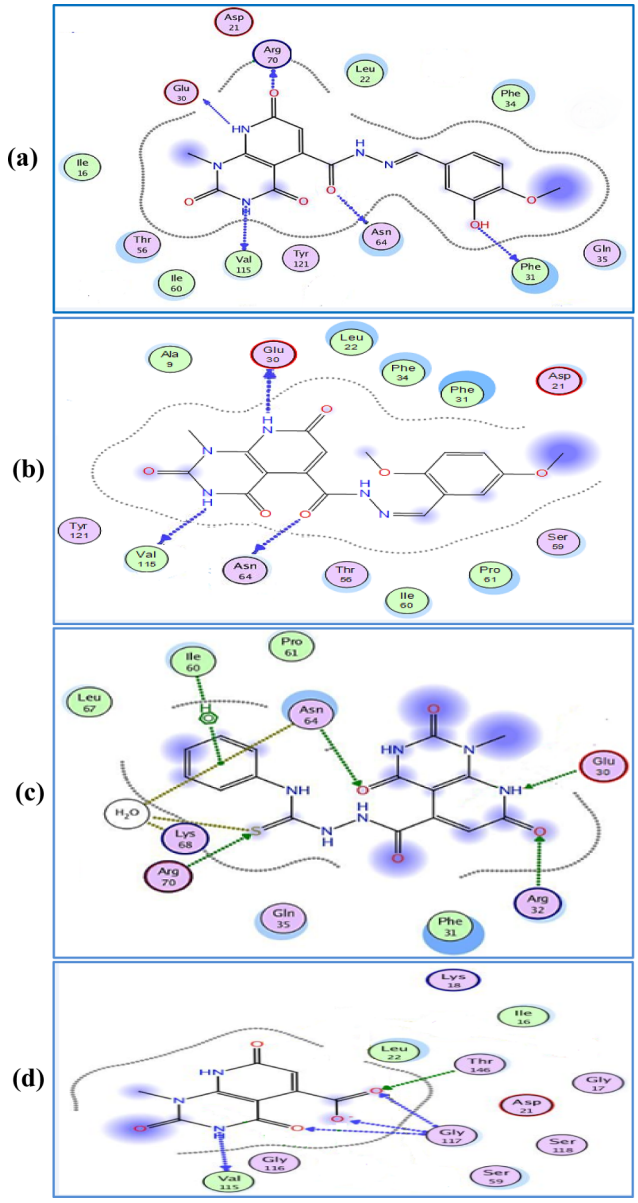

Fig. 5. 2D binding modes and residues involved in the recognition for the most active compounds docked and minimized in the DHFR binding pocket: (a) Compound 11 (IC_{50} = 6.5 μM); (b) Compound 13 (IC_{50} = 7.1 μM); (c) Compound 14 (IC_{50} = 8.7 μM); (d) Compound 3 (IC_{50} = 11.1 μM).

G2/M phase to 9.55% in comparison to the control cells (3.88%), which means that the cells were arrested at G2/M phase. On the other hand, G0/G1 population was 61.41% after treatment with compound **11**, when compared to the controlled cells 68.44%, suggesting that compound **11** might induce apoptosis in MCF-7 cells (Fig. 8A). An increase of apoptotic cell population was detected in treated MCF-7 cells with compound **11** for 24 h when compared with the untreated cells (Fig. 8B). This result indicates that compound **11** is an apoptotic inducer, which is consistent with the data obtained from cell cycle analysis in Fig. 8.

2.2.6. Detection and quantification of the levels of human active caspase-3 and caspase-9 proteins

To further clarify the exact signaling pathway involved in the apoptotic effects of compound **11**, we assessed the appropriate expression pattern of protein using human Caspase-3 and 9 ELISA. As shown in Table 5**.** Expression of both caspase-3 and 9 increased upon

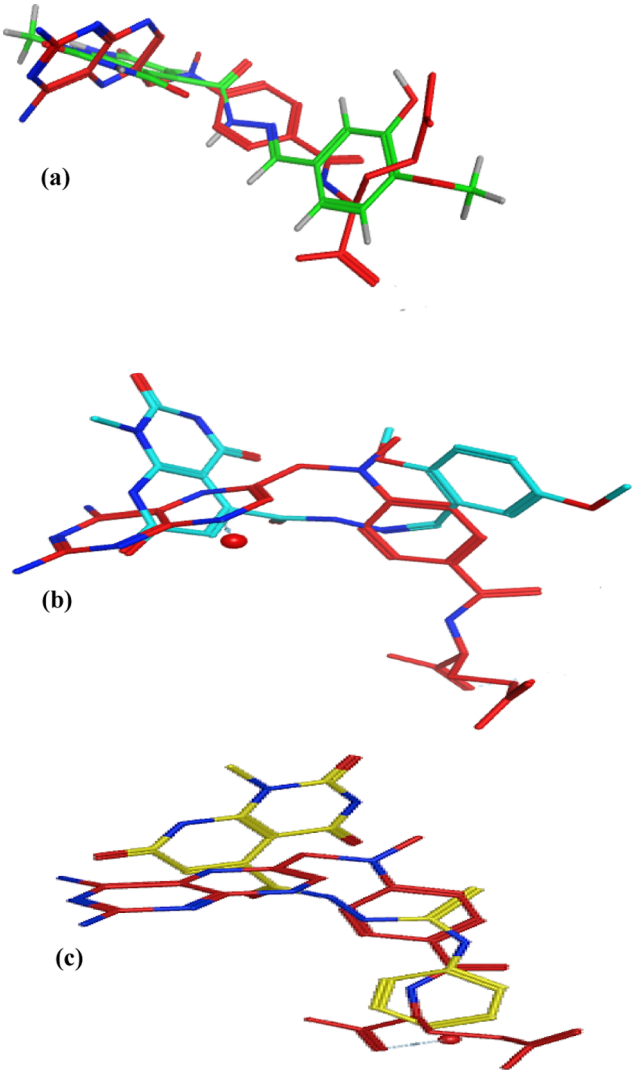

Fig. 6. Flexible alignment of the most active compounds: (a) Compound 11 (green); (b) Compound 13 (cyan); (c) Compound 14 (yellow); and MTX (red).

Table 4
Effect of compound 11 on the cell cycle progression in MCF-7 using flow cytometry.

Cell cycle arrest analysis in MCF-7 (μM/ml)				
	% G0/G1	% S	%G2/M	%Pre-G1
11	61.41	19.86	9.55	9.18
MTX	43.1	20.0	22.18	14.72
Control	68.44	26.97	3.88	0.71

treatment with compound **11** from 75 to 346.6 ng/ml and from 0.17 to 22.68 ng/mL, respectively.

3. Conclusion

A new series of pyrido[2,3-*d*]pyrimidines **3–18** was synthetized and found to have significant antitumor activity against five cancer lines. The target compounds **11**, **13** and **14** have shown the highest inhibitory activity towards DHFR. The molecular modeling study was done and confirmed the high potency of compounds **11**, **13** and **14**. Moreover, compound **11** also induced the process of apoptosis at Pre-G phase and cell cycle arrest at G2/M phase in MCF-7 cells.

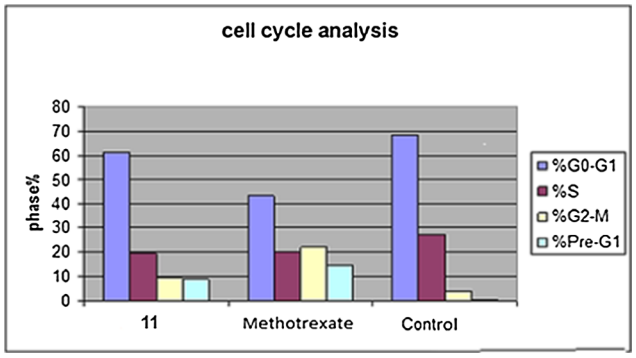

Fig. 7. Cell cycle arrest analysis of compound 11 in comparison with MTX.

4. Experimental

4.1. Chemistry

Melting points have been recorded using Stuart apparatus and are uncorrected. IR spectra have been recorded on Nicolet iS10FT-IR spectrometer (υ in cm^{-1}) using KBr discs. ^1H NMR and ^{13}C NMR spectra were recorded using Brurker 400 MHz and Joel 500 MHz in which tetramethylsilane (TMS) was used as internal standard. Mass spectrometry (EI or ESI) *m/z* analyses were performed on Hewlett Packard 5988 spectrometer or Advion compact mass spectrometer (CMS) NY | USA, respectively. The time of reaction has been determined using TLC technique on Silica gel plates 60 F245 E. Merk, and the spots have visualized by U.V. (366 nm). All chemicals have been purchased from Aldrich and used without further purification. Compound **2** was prepared according to the literature [17].

4.1.1. Synthesis of 1-methyl-2,4,7-trioxo-1,2,3,4,7,8-hexahydropyrido [2,3-d]pyrimidine-5-carboxylic acid (3).

To a suspension of methyl ester **2** (0.25 g, 1 mmol) in methanol (5 ml), NaOH (0.40 g, 0.01 mmol) was added at room temperature. The mixture was refluxed for about 4 h. When the reaction was completed as shown by TLC, the reaction mixture was cooled to room temperature, and the formed precipitate was filtered, washed with ethanol, dried, and recrystallized from acetone.

White solid, mp > 300 °C. Yield = 96%. IR (KBr, υ, cm^{-1}): 1659 (CO—NH), 1723 (CO—OH), 3312 (NH), 3455 (br, OH). ^1H NMR (500 MHz, DMSO-d_6): δ 3.42 (s, 3H, CH_3), 6.39 (s, 1H, C6-H), 11.52 (s, 1H, NH; D_2O exchangeable), 12.40 (s, 1H, COOH D_2O exchangeable). ^{13}C NMR (125 MHz, DMSO-d_6): δ 31.18, 102.88, 148.17, 151.03, 153.19, 160.10, 167.06, 168.44. EI-MS (*m/z*): 237.15 (M^+). Elemental analysis for $C_9H_7N_3O_5$, calcd.: C, 45.58; H, 2.97; N, 17.72. Found: C, 45.78; H, 2.85; N, 17.58.

Table 5
Effect of compound 11 on the levels of human caspase-3 and caspase-9.

Compound	Casp-3 (ng/ml)	fold	Casp-9 (ng/ml)	fold
11	346.6	4.62	22.68	31.8
MTX	521.3	6.95	28.18	39.6
Control	75	–	0.71	–

4.1.2. Synthesis of 1-methyl 2,4,7-trioxo-1,2,3,4,7,8- hexahydropyrido [2,3- d]pyrimidine-5-carbohydrazide (4).

To a suspension of the methyl carboxylate ester **2** (0.25 g, 1 mmol) in absolute ethanol (4 ml), hydrazine hydrate (0.10 g, 2 mmol) was added at room temperature and the reaction mixture was heated under reflux for 5 h. When the reaction was completed as shown by TLC, it was cooled to room temperature, and the produced precipitate was filtered, washed with ethyl acetate, and finally recrystallized from acetonitrile.

White solid, mp = 125–128 °C. Yield = 60%. IR (KBr, υ, cm^{-1}): 1680 (C═O), 3143 (NH), 3282, 3349 (NH_2). ^1H NMR (500 MHz, DMSO-d_6): δ 3.40 (s, 3H, CH_3), 5.67 (s, 1H, C6–H), 9.05 (s, 1H, NH; D_2O exchangeable), 11.13 (s, 2H, NH_2; D_2O exchangeable)

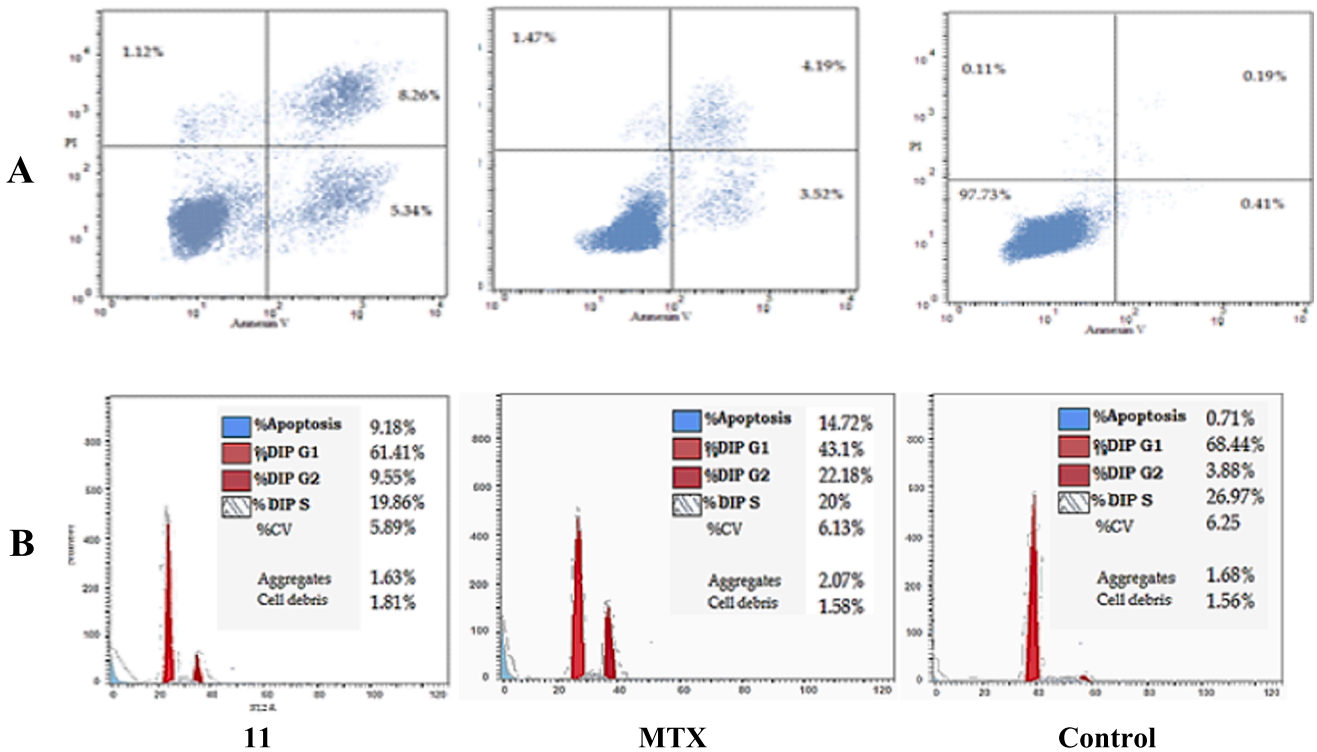

Fig. 8. Determination of apoptosis in MCF-7 cell line and cell cycle arrest with flow cytometry. (A) Effect of compound 11 on the cell cycle distribution of MCF-7cell line. (B) Apoptotic effect on human MCF-7 cell line induced by compound 11.

4.1.3. General procedure for the preparation of N-methyl N'-arylidene-2,4,7-trioxo-1,2,3,4,7,8 hexahydropyrido[2,3 d]pyrimidine-5-carbohydrazides (5–13)

To a suspension of hydrazide **4** (0.25 g, 1 mmol) in absolute ethanol (3 ml), aromatic aldehyde (2 mmol) was added. The reaction mixture was heated under reflux for 15 h. When the reaction was completed as shown by TLC, the reaction mixture was cooled to room temperature, the precipitated solid was collected by filtration, washed twice with ethyl acetate, carefully dried and recrystallized from acetonitrile. ^{1}H NMR spectra of all separated schiff bases showed two conformers in different ratios ranging from 1:1 to 1.8:1.

4.1.3.1. 1-Methyl N'-(3-nitrobenzylidene)-2,4,7-trioxo-1,2,3,4,7,8-hexahydropyrido[2,3-d] pyrimidine-5-carbohydrazide (5).. White solid, mp > 300 °C. Yield = 60%. IR (KBr, υ, cm^{-1}): 1353, 1529 (NO_2), 1564 (C═N), 1661 (CO-NH), 1682 (CO, hydrazide), 3083 (NH). The product was separated as a mixture of two conformers in ratio 3:2. For the **major conformer**: ^{1}H NMR (500 MHz, DMSO-d_6): δ 3.49 (s, 3H, CH_3), 6.39 (s, 1H, C6–H), 7.62 (t, J = 7.95 Hz, 1H, ArH), 7.79 (s, 1H, ArH), 8.09 (s, 1H, CH═N), 8.11 (s, 1H, ArH), 8.16 (s, 1H, ArH), 11.42 (s, 1H, NH; D_2O exchangeable), 12.19 (s, 1H, NH; D_2O exchangeable). For the **minor conformer**: ^{1}H NMR: δ 3.46 (s, 3H, CH_3), 6.45 (s, 1H, C6–H), 7.77 (d, J = 8.6 Hz, 1H, ArH), 8.14 (s, 1H, ArH), 8.18 (s, 1H, ArH), 8.28 (s, 1H, CH═N), 8.57 (s, 1H, ArH), 11.52 (s, 1H, NH; D_2O exchangeable), 11.94 (s, 1H, NH; D_2O exchangeable).

4.1.3.2. 1-Methyl N'-(4-nitrobenzylidene)-2,4,7-trioxo-1,2,3,4,7,8-hexahydropyrido[2,3-d] pyrimidine-5-carbohydrazide (6).. Yellow solid, mp > 300 °C. Yield = 84%. IR (KBr, υ, cm^{-1}): 1388, 1514 (NO_2), 1565 (C═N), 1629 (CO−NH), 1696 (CO, hydrazide), 3163 (NH). The product was separated as a mixture of two conformers in ratio 13:7. For the **major conformer**: ^{1}H NMR (500 MHz, DMSO-d_6): δ 3.47 (s, 3H, CH_3), 6.39 (s, 1H, C6-H), 7.58 (d, J = 8.7 Hz, 2H, ArH), 8.08 (s, 1H, CH═N), 8.17 (d, J = 8.7 Hz, 2H, ArH), 11.42 (s, 1H, NH; D_2O exchangeable), 12.23 (s, 1H, NH; D_2O exchangeable). For the **minor conformer**: ^{1}H NMR: δ = 3.45 (s, 3H, CH_3), 6.49 (s, 1H, C6-H), 7.99 (d, J = 8.7 Hz, 2H, ArH), 8.25 (s, 1H, CH═N), 8.31 (d, J = 8.7 Hz, 2H, ArH), 11.55 (s, 1H, NH; D_2O exchangeable), 11.97 (s, 1H, NH; D_2O exchangeable). ^{13}C NMR (125 MHz, DMSO-d_6): δ 29.04, 124.57, 127.95, 128.51, 140.70, 141.79, 144.98, 148.02, 149.82, 151.09, 152.94, 160.11, 163.56, 169.71. EI-MS (*m/z*): 284.11 (M^+). Elemental analysis for $C_{16}H_{12}N_6O_6$, calcd.: C, 50.01; H, 3.15; N, 21.87. Found: C, 50.25; H, 3.02; N, 21.68.

4.1.3.3. 1-Methyl N'-(4-flourobenzylidene)-2,4,7-trioxo-1,2,3,4,7,8-hexahydropyrido[2,3-d] pyrimidine-5-carbohydrazide (7).. White solid, mp > 300 °C. Yield = 79%. IR (KBr, υ, cm^{-1}): 1567 (C═N), 1665 (CO-NH), 1707 (CO, hydrazide), 3168 (NH). The product was separated as a mixture of two conformers in ratio 3:2. For the **major conformer**: ^{1}H NMR (500 MHz, DMSO-d_6): δ 3.46 (s, 3H, CH_3), 6.35 (s, 1H, C6-H), 7.16 (dd, J = 5.7, 8.5 Hz, 2H, ArH), 7.39 (dd, J = 5.7, 8.5 Hz, 2H, ArH), 7.96 (s, 1H, CH═N), 11.41 (s, 1H, NH; D_2O exchangeable), 11.92 (s, 1H, NH; D_2O exchangeable). For the **minor conformer**: ^{1}H NMR: δ 3.45 (s, 3H, CH_3), 6.45 (s, 1H, C6-H), 7.30 (t, dd, J = 5.7, 8.5 Hz, 2H, ArH), 7.78 (dd, J = 5.7, 8.5 Hz, 2H, ArH), 8.14 (s, 1H, CH═N), 11.52 (s, 1H, NH; D_2O exchangeable), 11.66 (s, 1H, NH; D_2O exchangeable). ^{13}C NMR (125 MHz, DMSO-d_6): δ 29.04, 100.33, 103.54, 116.45, 129.20, 131.04, 142.90, 146.33, 150.30, 152.90, 160.06, 162.04, 166.87, 169.29. ESI-MS (*m/z*): 356.1 ($M-H^+$), 357.1 (M^+). Elemental analysis for $C_{16}H_{12}FN_5O_4$, calcd.: C, 53.78; H, 3.39; N, 19.60. Found: C, 53.59; H, 3.21; N, 19.56.

4.1.3.4. 1-methyl N'-(4-hydroxybenzylidene)-2,7,7-trioxo-1,2,3,7,7,8-hexahydropyrido[2,3-d]pyrimidine-5-carbohydrazide (8).. White solid, mp > 300 °C. Yield = 66%. IR (KBr, υ, cm^{-1}): 1566 (C═N), 1653 (CO-NH), 1686 (CO, hydrazide), 2929 (NH), 3237 (OH). The product was separated as a mixture of two conformers in ratio 3:2. For the **major conformer**: ^{1}H NMR (500 MHz, DMSO-d_6): δ 3.45 (s, 3H, CH_3), 6.30 (s, 1H, C6–H), 6.69 (d, J = 8.6 Hz, 2H, ArH), 7.15 (d, J = 8.6 Hz, 2H, ArH). 7.85 (s, 1H, CH═N), 9.83 (s, 1H, OH; D_2O exchangeable), 11.38 (s, 1H, NH; D_2O exchangeable), 11.41 (s, 1H, NH; D_2O exchangeable), 11.68 (s, 1H, NH; D_2O exchangeable). For the **minor conformer**: ^{1}H NMR: δ = 3.43 (s, 3H, CH_3), 6.21 (s, 1H, C6–H), 6.82 (d, J = 8.6 Hz, 2H, ArH), 7.53 (d, J = 8.6 Hz, 2H, Ar-H), 8.02 (s, 1H, CH═N), 9.95 (s, 1H, OH; D_2O exchangeable).

4.1.3.5. 1-methyl N'-(4-N,N dimethyl aminobenzyidenel)-2,4,7-trioxo-1,2,3,4,7,8 hexahydro- pyrido[2,3-d]pyrimidine-5-carbohydrazide (9). White solid, mp > 300 °C. Yield = 70%. IR (KBr, υ, cm^{-1}): 1569 (C═N), 1601 (CO-NH), 1693(CO, hydrazide), 3029 (NH). The product was separated as a mixture of two conformers in ratio 1:1. For the **major conformer**: ^{1}H NMR (500 MHz, DMSO-d_6): δ 2.90 (s, 6H, $2CH_3$), 3.47 (s, 3H, CH_3), 6.31(s, 1H, C6–H), 6.63 (d, J = 8.9 Hz, 2H, ArH), 6.76 (d, J = 8.9 Hz, 2H, ArH), 7.82 (s, 1H, CH═N), 11.31 (s, 1H, NH; D_2O exchangeable), 11.37 (s, 1H, NH; D_2O exchangeable), 11.60 (s, 1H, NH; D_2O exchangeable). For the **minor conformer**: ^{1}H NMR: δ 2.98 (s, 6H, $2CH_3$), 3.44 (s, 3H, CH_3), 6.21 (s, 1H, C6–H), 7.14 (d, J = 8.9 Hz, 2H, ArH), 7.52 (d, J = 8.9 Hz, 2H, ArH), 7.99 (s, 1H, CH═N).

4.1.3.6. 1-Methyl N'-(4-flouro 2-methoxy, benzylidene)-2,4,7-trioxo-1,2,3,4,7,8-hexahydro- pyrido[2,3-d]pyrimidine-5-carbohydrazide (10). White solid, mp > 300 °C. Yield = 68%. IR (KBr, υ, cm^{-1}): 1282 (C−O), 1565 (C═N), 1642 (CO-NH), 1693 (CO, hydrazide), 3053 (NH). The product was separated as a mixture of two conformers in ratio 1:1. For the **major conformer**: ^{1}H NMR (500 MHz, DMSO-d_6): δ 3.45 (s, 3H, CH_3), 3.74 (s, 3H, OCH_3), 6.33 (s, 1H, C6-H), 6.73 (dd, J = 2.3, 8.8 Hz, 1H, ArH), 6.91 (s, 1H, ArH), 7.20 (t, J = 8.7 Hz, 1H, ArH), 8.08 (s, 1H, CH═N), 11.38 (s, 1H, NH; D_2O exchangeable), 11.85 (s, 1H, NH; D_2O exchangeable). For the **minor conformer**: ^{1}H NMR: δ 3.44 (s, 3H, CH_3), 3.82 (s, 3H, OCH_3), 6.39 (s, 1H, C6-H), 6.85 (dd, J = 2.3, 8.8 Hz, 1H, ArH), 6.93 (s, 1H, ArH), 7.85 (t, J = 8.7 Hz, 1H, ArH), 8.28 (s, 1H, CH═N), 11.44 (s, 1H, NH; D_2O exchangeable), 11.60 (s, 1H, NH; D_2O exchangeable). ESI-MS (*m/z*): 386.10 ($M-H^+$), 357.10 (M^+). Elemental analysis for $C_{17}H_{14}FN_5O_5$, calcd.: C, 52.72; H, 3.64; N, 18.08. Found: C, 52.83; H, 3.75; N, 18.38.

4.1.3.7. 1-Methyl N'-(3-hydroxy, 4-methoxybenzylidene)-2,4,7-trioxo-1,2,3,4,7,8-hexahydro- pyrido[2,3-d]pyrimidine-5-carbohydrazide (11). White solid, mp > 300 °C. Yield = 85%. IR (KBr, υ, cm^{-1}): 1266 (C−O), 1577 (C═N), 1649 (CONH), 1715 (CO, hydrazide), 3131 (OH), 3169 (NH). The product was separated as a mixture of two conformers in ratio 3:2. For the **major conformer**: (500 MHz, DMSO-d_6) ^{1}H NMR δ 3.47 (s, 3H, CH_3), 3.73 (s, 3H, OCH_3), 6.35 (s, 1H, C6–H), 6.72 (d, J = 1.7 Hz, 1H, ArH), 6.77 (dd, J = 1.7, 8.3 Hz, 1H, ArH), 6.86 (d, J = 8.3 Hz, 1H, ArH), 7.81 (s, 1H, CH═N), 9.17 (s, 1H, OH; D_2O exchangeable), 11.41 (s, 1H, NH; D_2O exchangeable), 11.71 (s, 1H, NH; D_2O exchangeable). For the **minor conformer**: ^{1}H NMR: δ 3.45 (s, 3H, CH_3), 3.80 (s, 3H, OCH_3), 6.44 (s, 1H, C6– H), 6.97 (d, J = 8.3 Hz, 1H, ArH), 7.03 (dd, J = 1.7, 8.3 Hz, 1H, ArH), 7.24 (d, J = 1.7 Hz, 1H, ArH), 7.97 (s, 1H, CH═N), 9.32 (s, 1H, OH; D_2O exchangeable), 11.45 (s, 1H, NH; D_2O exchangeable), 11.51 (s, 1H, NH; D_2O exchangeable). ^{13}C NMR (100 MHz, DMSO-d_6): δ 29.04, 55.94, 100.31, 103.54, 104.97, 112.24, 120.33, 127.55, 144.27, 147.31, 149.23, 151.05, 153.27, 160.01, 162.88, 166.87, 168.95.

4.1.3.8. 1-methyln'-(3,4-dimethoxybenzylidene)-2,4,7-trioxo-1,2,3,4,7,8-hexahydro pyrido- [2,3-d]pyrimidine-5-carbohydrazide (12). Yellow solid, mp > 300 °C. Yield = 72%. IR (KBr, υ, cm^{-1}): 1268 (C−O),1575 (C═N), 1667 (CO-NH), 1722 (C═O) 3169 (NH). The product was separated as a mixture of two conformers in ratio 11:9. For

the **major conformer**: ^{1}H NMR (500 MHz, DMSO-d_6): δ 3.45 (s, 3H, CH_3), 3.55 (s, 3H, OCH_3), 3.72 (s, 3H, OCH_3), 6.37 (s, 1H, C6-H), 6.79 (s, 1H, ArH), 6.91 (s, 1H, ArH), 7.02 (d, J = 7.9 Hz, 1H, ArH), 7.84 (s, 1H, CH=N), 11.43 (s, 1H, NH; D_2O exchangeable), 11.80 (s, 1H, NH; D_2O exchangeable). For the **minor conformer**: ^{1}H NMR: δ = 3.44 (s, 3H, CH_3), 3.80 (s, 3H, OCH_3), 3.82 (s, 3H, OCH_3), 6.43 (s, 1H, C6-H), 6.90 (s, 1H, ArH), 7.18 (d, J = 7.9 Hz, 1H, ArH), 7.34 (s, 1H, ArH), 8.05 (s, 1H, CH=N), 11.49 (s, 1H, NH; D_2O exchangeable), 11.52 (s, 1H, NH; D_2O exchangeable).

4.1.3.9. 1-Methyl N'-(2,5-dimethoxybenzylidene)-2,4,7-trioxo-1,2,3,4,7,8-hexahydropyrido- [2,3-d]pyrimidine-5-carbohydrazide (13). White solid, mp > 300 °C. Yield = 81%. IR (KBr, υ, cm^{-1}): 1226 (C—O), 1573 (C=N), 1631 (CO-NH), 1691 (CO, hydrazide), 3160 (NH). The product was separated as a mixture of two conformers in ratio 13:7. For the **major conformer**: ^{1}H NMR (500 MHz, DMSO-d_6): δ 3.44 (s, 3H, CH_3), 3.50 (s, 3H, OCH_3), 3.75 (s, 3H, OCH_3), 6.36 (s, 1H, C6-H), 6.62 (d, J = 3 Hz, 1H, ArH), 6.89 (dd, J = 3.2, 9.0 Hz, 1H, ArH), 7.11 (s, 1H, ArH), 8.19 (s, 1H, CH=N), 11.43 (s, 1H, NH; D_2O exchangeable), 11.85(s, 1H, NH; D_2O exchangeable). For the **minor conformer**: ^{1}H NMR: δ = 3.77 (s, 3H, CH_3-N), 3.79 (s, 3H, OCH_3), 3.84 (s, 3H, OCH_3), 6.42 (s, 1H, C6-H), 7.01 (dd, J = 3.2, 9.0 Hz, 1H, ArH), 7.36, (d, J = 3 Hz, 1H, ArH), 7.49 (s, 1H, ArH), 8.46 (s, 1H, CH=N), 11.49 (s, 1H, NH; D_2O exchangeable), 11.60 (s, 1H, NH; D_2O exchangeable). ^{13}C NMR (125 MHz, DMSO-d_6): δ 28.95, 55.16, 56.61, 109.22, 110.21, 113.80, 117.35, 118.37, 120.00, 123.16, 138.91, 142.93, 151.06, 157.03, 160.07, 163.00, 166.95, 169.26. EI-MS (m/z): 399.21 (M^+). Elemental analysis for $C_{18}H_{17}N_5O_6$, calcd.: C, 54.14; H, 4.29; N, 17.54. Found: C, 54.33; H, 4.38; N, 17.39.

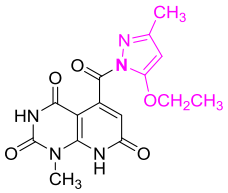

4.1.4. General procedure for the preparation of N-aryl (1-methyl-2,4,7-trioxo-1,2,3,4,7,8-hexahydropyrido[2,3-d]pyrimidine)-5-carbohydrazinocarbothioamides (14, 15)

To a suspension of **4** (0.75 g, 3 mmol) in DMF (5 ml), appropriate aryl isothiocyanate (3 mmol) was added. The reaction mixture was stirred at room temperature and the time of the reaction was monitored by TLC. Then, it was poured into crushed ice and the solid formed was filtered, dried and recrystallized from *n*-hexane.

4.1.4.1. Synthesis of N-phenyl (1-methyl-2,4,7-trioxo-1,2,3,4,7,8-hexahydropyrido[2,3-d]pyrimidine)-5-carbohydrazinocarbothioamide (14). White solid, mp > 300 °C. Yield = 91%. %. IR (KBr, υ, cm^{-1}): 1287 (C=S), 1678 (C=O), 3195, 3276 (NH). ^{1}H NMR (400 MHz, DMSO-d_6): δ 3.45 (s, 3H, CH_3), 6.33 (s, 1H, C6-H), 7.17 (s, 1H, ArH), 7.34 (s, 2H, ArH), 7.73 (s, 2H, ArH), 9.78 (s, 1H, NH; D_2O exchangeable), 9.99 (s, 1H, NH; D_2O exchangeable), 10.64 (s, 1H, NH; D_2O exchangeable), 11.86 (s, 1H, NH; D_2O exchangeable). ^{13}C NMR (100 MHz, DMSO-d_6): δ 29.13, 105.27, 124.77, 125.33, 128.58, 139.53, 147.80, 150.72, 153.67, 161.63, 166.45, 167.69, 180.85. EI-MS (m/z): 386.44 (M^+). Elemental analysis for $C_{16}H_{14}N_6O_4S$, calcd.: C, 49.74; H, 3.65; N, 21.75; S, 8.30. Found: C, 49.81; H, 3.57; N, 21.99; S, 8.37.

4.1.4.2. Synthesis of N-4′-nitrophenyl (1-methyl-2,4,7-trioxo-1,2,3,4,7,8-hexahydro pyrido [2,3-d]pyrimidine)-5-carbohydrazinocarbothioamide (15). Orange solid, mp > 300 °C. Yield = 70%. IR (KBr, υ, cm^{-1}): 1325 (C=S), 1689 (C=O), 3215, 3285 (NH). ^{1}H NMR (400 MHz, DMSO-d_6): δ 3.45 (s, 3H, CH_3), 6.30 (s, 1H, C6-H), 8.20 (d, J = 8.9 Hz, 2H, ArH), 8.35 (d, J = 8.9 Hz, 2H, ArH), 10.25 (s, 1H, NH; D_2O exchangeable), 10.42 (s, 1H, NH; D_2O exchangeable), 10.66 (s, 1H, NH; D_2O exchangeable), 11.9 (s, 1H, NH; D_2O exchangeable).

4.1.5. General procedure for the preparation 5-(3,5- disubstituted 1-carbonyl-1H-pyrazole)-1-methylpyrido[2,3-d]pyrimidine-2,4,7(1H,3H,8H)-triones (16–18)

To a suspension of hydrazide **4** (0.75 g, 3 mmol) in absolute ethanol (20 ml), the appropriate 1,3-dicarbonyl compound (6 mmol) was added. The reaction mixture was heated under reflux for 18 h. The obtained solid was filtered, washed well with ethanol, then dried, and recrystallized from *n*-hexane.

4.1.5.1. Synthesis of 5-(3,5-dimethyl 1-carbonyl-1H-pyrazole)-1-methylpyrido[2,3-d] pyrim- dine-2,4,7(1H,3H,8H)-trione (16). White solid, mp > 300 °C. Yield = 69%. IR (KBr, υ, cm^{-1}): 1577 (C=N), 1655 (C=O), 2999, 3130 (NH). ^{1}H NMR (400 MHz, DMSO-d_6): δ 2.04 (s, 3H, CH_3, pyrazole), 2.59 (s, 3H, CH_3, pyrazole), 3.46 (s, 3H, CH_3), 6.23 (s, 1H, C6-H), 6.55 (s, 1H, CH, pyrazole), 11.49 (s, 1H, NH; D_2O exchangeable). ^{13}C NMR (100 MHz, DMSO-d_6): δ 13.90, 14.08, 28.95, 100.06, 104.02, 111.77, 143.96, 148.49, 151.05, 152.67, 152.86, 160.13, 167.22. ESI-MS (m/z): 314.1 ($M-H^+$), 315.0 (M^+). Elemental analysis for $C_{14}H_{13}N_5O_4$, calcd.: C, 53.33; H, 4.16; N, 22.21;. Found: C, 53.12; H, 4.34; N, 22.43.

4.1.5.2. Synthesis of 5-(5-ethoxy-3-methyl-1-carbonyl-1H-pyrazole)-1-methylpyrido[2,3-d] pyrimidine-2,4,7(1H,3H,8H)-trione (17)

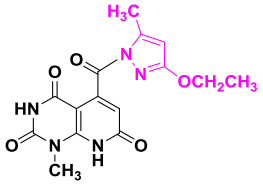

Yellow solid, mp > 300 °C. Yield = 76%. IR (KBr, υ, cm^{-1}): 1576 (C=N), 1696 (C=O), 3037, 3225 (NH). It is present as two regioisomers in ratio (6:4). For the **first regioisomer:** ^{1}H NMR (400 MHz, DMSO-d_6): δ 1.03 (t, J = 7 Hz, 3H, $OCH_2\underline{CH_3}$), 1.87 (s, 3H, CH_3, pyrazole), 3.55 (s, H, CH_3), 3.77 (dd, J = 7, 12 Hz, 2H, $O\underline{CH_2}CH_3$), 6.16 (s, 1H, C6-H), 6.49(s, 1H, pyrazole), 10.93 (s, 1H, NH; D_2O exchangeable), 11.39 (s, 1H, NH; D_2O exchangeable). For the **second regioisomer**: ^{1}H NMR: δ 1.22 (t, J = 7 Hz, 3H, $OCH_2\underline{CH_3}$), 3.05 (s, 3H, CH_3, pyrazole), 3.61(s, 3H, CH_3), 4.12 (dd, J = 7, 12 Hz, 2H, $O\underline{CH_2}CH_3$), 6.24 (s, 1H, C6-H), 10.52 (s, 1H, NH; D_2O exchangeable), 11.49 (s, 1H, NH; D_2O exchangeable). ^{13}C NMR (100 MHz, DMSO-d_6): δ = 13.90, 14.08, 28.95, 100.06, 104.02, 111.77, 143.96, 148.49, 151.05, 152.67, 152.86, 160.13, 167.22.

4.1.5.3. Synthesis of 1-methyl-5-(3-methyl-5-phenyl-1-carbonyl-1H-pyrazole)pyrido[2,3-d] pyrimidine-2,4,7(1H,3H,8H)-trione (18). White solid, mp > 300 °C. Yield = 79%. IR (KBr, υ, cm^{-1}): 1575 (C=N), 1677 (C=O), 3214, 3328 (NH). ^{1}H NMR (400 MHz, DMSO-d_6): δ 1.85 (s, 3H, CH_3, pyrazole), 3.45 (s, 3H, CH_3), 6.23 (s, 1H, C6-H), 7.15 (s, 1H, CH, pyrazole), 7.26 (dd, J = 7.5, 7.5 Hz, 1H, ArH), 7.32 (d, J = 7.5 Hz, 1H, ArH), 7.39 (dd, J = 7.5, 7.5 Hz, 1H, ArH), 7.47 (d, J = 7.8 Hz, 1H, ArH), 7.75 (d, J = 7.5 Hz, 1H, ArH), 11.52 (s, 1H, NH; D_2O exchangeable), 12.24 (s, 1H, NH; D_2O exchangeable). ^{13}C NMR (100 MHz, DMSO-d_6): δ 16.04, 29.06, 56.5, 92.3, 103.27, 124.94,

125.75, 127.45, 128.5, 143.69, 151.11, 153.02, 155.19, 160.21, 163.55, 166.84. EI-MS (*m/z*): 377.02 (M^+). Elemental analysis for $C_{19}H_{15}N_5O_4$, calcd.: C, 60.47; H, 4.01; N, 18.56. Found: C, 60.61; H, 4.32; N, 18.45.

4.2. Biological assay

4.2.1. Cytotoxicity screening using MTT assay

All the newly synthetized compounds were assessed for their *in vitro* antitumor activity using the standard MTT technique of tetrazolium salt (3-(4,5-dimethyl-2-thiazolyl)-2,5-diphenyl-2H-tetrazolium bromide) against five human tumor cell lines [42,43]. The cytotoxic activity was defined as the concentration of the compound that causes 50% growth inhibition compared with the growth of untreated cells.

4.2.2. Human DHFR enzyme inhibition assay.

DHFR activity was verified by enzyme-linked immunosorbent assay (ELISA) assay technique. The assay exploited a specific antibody for human DHFR firmly coated on a 96-well plate, in which 100 ml of the standard solution or the tested compounds were added to every well at room temperature. Then, the mean absorbance of each group of standard and tested compounds was determined. The standard curve was drawm on log-log paper with the absorbance on the Y-axis and the standard concentration on the X-axis. Percent Inhibition was assesed through comparing both test compounds and control results, whereas IC_{50} was assesd from concentration/inhibition curve using MTX as a standard [44].

4.2.3. Cell cycle arrest analysis

To perform flow cytometric analysis of the content of DNA, MCF-7 cells in exponential growth were mixed with compound **11** and incubated for a period of 24 h. The cells were gathered, centrifuged and fixed well with ice cold ethanol (70%). The cells were also treated with an important buffer containing RNAse A and 0.1% Triton X-100, then stained completely with propidum iodide and compared with the control which was also mixed with DMSO. DNA contents were accurately measured by flow cytometry technique [45].

4.2.4. Detection of the levels of human active caspase-3 and caspase-9 proteins

Sandwich enzyme linked immunosorbent assay was used to determine level of human active caspase-3. Tested compounds were carefully added to the cells and lysed using cell extraction buffer. Incubation at room temperature for 4 h was followed by washing of wells for 4 times, after that, 100 μL of Invitrogen Caspase-3 (active) monoclonal antibody solution was added and incubated once more at room temperature for 2 h. Wells were precisely washed for 4 times, and the wells were incubated for 30 min at room temperature after the addition of (100 μL) of solutiton named as anti-Rabbit IgG horseradish peroxidase (HRP). After washing again, the chromogen was added. Finally, absorbance was measured at 450 nm. Similar procedure was used for determination of caspase-9 using Invitrogen Caspase-9 (active) Human ELISA kit [46].

4.3. Molecular modeling methodology

4.3.1. Enzyme structure

Starting with the complex of DHFR and MTX (PDB code 1U72) which was obtained from the RCSB Protein Data Bank [34–37] and MOE software version 2014.09 was used to define the 2D ligand interaction of MTX and DHFR (Fig. 4).

4.3.2. Molecular structure of selected compounds

The four DHFR inhibitors (**3, 11**, **13** and **14**) were constructed from fragment library in the MOE program followed by energy minimization using the "Amber force field". The partial atomic charges for each analogue were assigned with the semiemperical mechanical calculation method "AM1″ implanted in MOE.

4.3.3. Conformational search and the derived structural global minima

The partially charged and energy minimized structures of the tested compounds were subjected to stochastic conformational search using the stochastic conformational search module implemented in MOE. The conformers with the lowest energy were selected as the global minimal for further modeling studies.

Appendix A. Supplementary material

Supplementary data to this article can be found online at https://doi.org/10.1016/j.bioorg.2019.103076.

References

[1] K. Misselbeck, L. Marchetti, M.S. Field, M. Scotti, C. Priami, P.J. Stover, A hybrid stochastic model of folate-mediated one-carbon metabolism: Effect of the common C677T MTHFR variant on de novo thymidylate biosynthesis, Sci. Rep. 7 (2017) 797.

[2] T.C. Alexander, C.M. Simecka, F. Kiffer, T. Groves, J. Anderson, H. Carr, J. Wang, G. Carter, A.R. Allen, Changes in cognition and dendritic complexity following intrathecal methotrexate and cytarabine treatment in a juvenile murine model, Behav. Brain Res. 346 (2018) 21–28.

[3] L.H. Matherly, Molecular and cellular biology of the human reduced folate carrier, Prog. Nucleic Acid Res. Mol. Biol. 67 (2001) 131–162.

[4] A. Gangjee, H.D. Jain, S. Kurup, Recent advances in classical and non-classical antifolates as antitumor and antiopportunistic infection agents: Part II, Anti-Cancer Agents in Medicinal, Chem. (Formerly Curr. Med. Chem.-Anti-Cancer Agents) 8 (2008) 205–231.

[5] H. Li, F. Fang, Y. Liu, L. Xue, M. Wang, Y. Guo, X. Wang, C. Tian, J. Liu, Z. Zhang, Inhibitors of dihydrofolate reductase as antitumor agents: design, synthesis and biological evaluation of a series of novel nonclassical 6-substituted pyrido [3, 2-d] pyrimidines with a three-to five-carbon bridge, Bioorg. Med. Chem. 26 (2018) 2674–2685.

[6] M. Wang, J. Yang, M. Yuan, L. Xue, H. Li, C. Tian, X. Wang, J. Liu, Z. Zhang, Synthesis and antiproliferative activity of a series of novel 6-substituted pyrido [3, 2-d] pyrimidines as potential nonclassical lipophilic antifolates targeting dihydrofolate reductase, Eur. J. Med. Chem. 128 (2017) 88–97.

[7] V. Cody, C.H. Schwalbe, Structural characteristics of antifolate dihydrofolate reductase enzyme interactions, Crystallogr. Rev. 12 (2006) 301–333.

[8] T. Itoh, N. Hatae, T. Nishiyama, T. Choshi, S. Hibino, T. Yoshimura, M. Ishikura, Synthesis and cytotoxicity of pyrido [4, 3-b] carbazole alkaloids against HCT-116 and HL-60 cells, Med. Chem. Res. 27 (2018) 412–419.

[9] M. Zink, H. Lanig, R. Troschütz, Structural variations of piritrexim, a lipophilic inhibitor of human dihydrofolate reductase: synthesis, antitumor activity and molecular modeling investigations, Eur. J. Med. Chem. 39 (2004) 1079–1088.

[10] V. Cody, J. Pace, Structural analysis of Pneumocystis carinii and human DHFR complexes with NADPH and a series of five potent 6-[5′-(ω-carboxyalkoxy) benzyl] pyrido [2, 3-d] pyrimidine derivatives, Acta Crystallogr. Sect. D: Biol. Crystallogr. 67 (2011) 1–7.

[11] B.M. Spowage, C.L. Bruce, J.D. Hirst, Interpretable correlation descriptors for quantitative structure-activity relationships, J. Cheminformat. 1 (2009) 22.

[12] J.R. Piper, C.A. Johnson, C.A. Krauth, R.L. Carter, C.A. Hosmer, S.F. Queener, S.E. Borotz, E.R. Pfefferkorn, Lipophilic antifolates as agents against opportunistic infections. 1. Agents superior to trimetrexate and piritrexim against Toxoplasma gondii and Pneumocystis carinii in in vitro evaluations, J. Med. Chem. 39 (1996) 1271–1280.

[13] D. Chan, A. Anderson, Towards species-specific antifolates, Curr. Med. Chem. 13 (2006) 377–398.

[14] A. Gangjee, R. Devraj, S.F. Queener, Synthesis and dihydrofolate reductase inhibitory activities of 2, 4-diamino-5-deaza and 2, 4-diamino-5, 10-dideaza lipophilic antifolates, J. Med. Chem. 40 (1997) 470–478.

[15] R.G. Nelson, A. Rosowsky, Dicyclic and tricyclic diaminopyrimidine derivatives as potent inhibitors of Cryptosporidium parvum dihydrofolate reductase: structure-activity and structure-selectivity correlations, Antimicrob. Agents Chemother. 45 (2001) 3293–3303.

[16] S. Karabulut, N. Sizochenko, A. Orhan, J. Leszczynski, A DFT-based QSAR study on inhibition of human dihydrofolate reductase, J. Mol. Graph. Model. 70 (2016) 23–29.

[17] A. Shamroukh, A. Rashad, F. Abdelmegeid, The chemistry of pyrido [2, 3-d] pyrimidines and their applications, J. Chem. Pharmaceut. Res. 8 (2016) 734–772.

[18] W. Dong, J. Xu, L. Xiong, X. Liu, Z. Li, Synthesis, structure and biological activities of some novel anthranilic acid esters containing N-pyridylpyrazole, Chin. J. Chem. 27 (2009) 579–586.

[19] P. Cui, X. Li, M. Zhu, B. Wang, J. Liu, H. Chen, Design, synthesis and antimicrobial activities of thiouracil derivatives containing triazolo-thiadiazole as SecA inhibitors, Eur. J. Med. Chem. 127 (2017) 159–165.

[20] R.U. Ambhure, S.R. Mirgane, D.U. Thombal, R.B. Nawale, R.P. Marathe, R.P. Pawar, Synthesis and antibacterial study of some schiff bases complexes, Modern Organic

Chem. Res. 2 (2017) 11.
[21] O.O. Ajani, C.A. Obafemi, O.C. Nwinyi, D.A. Akinpelu, Microwave assisted synthesis and antimicrobial activity of 2-quinoxalinone-3-hydrazone derivatives, Bioorg. Med. Chem. 18 (2010) 214–221.
[22] J. Patole, U. Sandbhor, S. Padhye, D.N. Deobagkar, C.E. Anson, A. Powell, Structural chemistry and in vitro antitubercular activity of acetylpyridine benzoyl hydrazone and its copper complex against Mycobacterium smegmatis, Bioorg. Med. Chem. Lett. 13 (2003) 51–55.
[23] G. Palla, C. Pelizzi, G. Predieri, C. Vignali, Conformational study on N-acylhydrazones of aromatic-aldehydes by nmr-spectroscopy, SOC CHIMICA ITALIANA VIALE LIEGI 48, I-00198 ROME, ITALY, 1982, pp. 339–341.
[24] G. Palla, G. Predieri, P. Domiano, C. Vignali, W. Turner, Conformational behaviour and E/Z isomerization of N-acyl and N-aroylhydrazones, Tetrahedron 42 (1986) 3649–3654.
[25] A.B. Lopes, E. Miguez, A.E. Kümmerle, V.M. Rumjanek, C.A.M. Fraga, E.J. Barreiro, Characterization of amide bond conformers for a novel heterocyclic template of N-acylhydrazone derivatives, Molecules 18 (2013) 11683–11704.
[26] M. Seelam, P.R. Kammela, B. Shaikh, R. Tamminana, S. Bogiri, Cobalt-promoted one-pot reaction of isothiocyanates toward the synthesis of aryl/alkylcyanamides and substituted tetrazoles, Chem. Heterocycl. Compd. 54 (2018) 535–544.
[27] G. Khalili, A mild one-pot synthesis of S-aryl carbamimidothioates using diazonium salts under catalyst-free condition, Monatshefte für Chemie-Chemical Monthly 146 (2015) 1891–1894.
[28] G. Hossain, M. Abedin, S.C. Bachar, Synthesis and characterization of N1-phenylhydrazine-1, 2-bis (carbothioamide) and its evaluation for antimicrobial, antioxidant, and brine shrimp lethality bioassay, Organic Chem. Int. 2012 (2012).
[29] S.C. Karad, V.B. Purohit, P. Thakor, V.R. Thakkar, D.K. Raval, Novel morpholinoquinoline nucleus clubbed with pyrazoline scaffolds: Synthesis, antibacterial, antitubercular and antimalarial activities, Eur. J. Med. Chem. 112 (2016) 270–279.
[30] R.S. Joshi, P.G. Mandhane, S.D. Diwakar, S.K. Dabhade, C.H. Gill, Synthesis, analgesic and anti-inflammatory activities of some novel pyrazolines derivatives, Bioorg. Med. Chem. Lett. 20 (2010) 3721–3725.
[31] A.V. Zerov, T.S. Krupenya, A.A. Petrov, S.I. Yakimovich, Reaction of trifluoromethyl-containing 1,3-dicarbonyl compounds with bis-hydrazides, Russ. J. Org. Chem. 52 (2016) 312–318.
[32] S.S. Kamble, G.S. Shankarling, A unique blend of water DES and ultrasound for One-Pot Knorr pyrazole synthesis and knoevenagel-michael addition reaction, ChemistrySel. 3 (2018) 2032–2036.
[33] G. Rastelli, S. Pacchioni, W. Sirawaraporn, R. Sirawaraporn, M.D. Parenti, A.M. Ferrari, Docking and database screening reveal new classes of plasmodium f alciparum dihydrofolate reductase inhibitors, J. Med. Chem. 46 (2003) 2834–2845.
[34] V. Cody, Structural analysis of dihydrofolate reductase and thymidylate synthase from mammalian and pathogenic organisms, Curr. Enzym. Inhib. 8 (2012) 124–139.
[35] M. Arooj, S. Sakkiah, G. Cao, K.W. Lee, An innovative strategy for dual inhibitor design and its application in dual inhibition of human thymidylate synthase and dihydrofolate reductase enzymes, PLoS One 8 (2013) e60470.
[36] J.P. Volpato, E. Fossati, J.N. Pelletier, Increasing methotrexate resistance by combination of active-site mutations in human dihydrofolate reductase, J. Mol. Biol. 373 (2007) 599–611.
[37] P.T. Wong, S.K. Choi, Mechanisms and implications of dual-acting methotrexate in folate-targeted nanotherapeutic delivery, Int. J. Mol. Sci. 16 (2015) 1772–1790.
[38] S.T. Al-Rashood, I.A. Aboldahab, M.N. Nagi, L.A. Abouzeid, A.A. Abdel-Aziz, S.G. Abdel-hamide, K.M. Youssef, A.M. Al-Obaid, H.I. El-Subbagh, Synthesis, dihydrofolate reductase inhibition, antitumor testing, and molecular modeling study of some new 4 (3H)-quinazolinone analogs, Bioorg. Med. Chem. 14 (2006) 8608–8621.
[39] G.S. Hassan, S.M. El-Messery, F.A. Al-Omary, S.T. Al-Rashood, M.I. Shabayek, Y.S. Abulfadl, E.-S.E. Habib, S.M. El-Hallouty, W. Fayad, K.M. Mohamed, Nonclassical antifolates, part 4. 5-(2-Aminothiazol-4-yl)-4-phenyl-4H-1, 2, 4-triazole-3-thiols as a new class of DHFR inhibitors: Synthesis, biological evaluation and molecular modeling study, Eur. J. Med. Chem. 66 (2013) 135–145.
[40] A. Heifets, R.H. Lilien, LigAlign: flexible ligand-based active site alignment and analysis, J. Mol. Graph. Model. 29 (2010) 93–101.
[41] S. Fares, K.B. Selim, M.A. El-Sayed, F.E. Goda, Synthesis, biological evaluation and molecular modeling of novel benzofuran-N-heterocyclic hybrids as anticancer agents, J. Am. Sci. 13 (2017).
[42] M.S. Karbownik, J. Szemraj, Ł. Wieteska, A. Antczak, P. Górski, E. Kowalczyk, T. Pietras, Antipsychotic drugs differentially affect mRNA expression of genes encoding the neuregulin 1-downstream ErbB4-PI3K pathway, Pharmacology 98 (2016) 4–12.
[43] M.A.-A. El-Sayed, W.M. El-Husseiny, N.I. Abdel-Aziz, A.S. El-Azab, H.A. Abuelizz, A.A.-M. Abdel-Aziz, Synthesis and biological evaluation of 2-styrylquinolines as antitumour agents and EGFR kinase inhibitors: molecular docking study, J. Enzyme Inhib. Med. Chem. 33 (2018) 199–209.
[44] J.J. Priola, N. Calzadilla, M. Baumann, N. Borth, C.G. Tate, M.J. Betenbaugh, High-throughput screening and selection of mammalian cells for enhanced protein production, Biotechnol. J. 11 (2016) 853–865.
[45] T.M. Thornton, M. Rincon, Non-classical p38 map kinase functions: cell cycle checkpoints and survival, Int. J. Biol. Sci. 5 (2009) 44.
[46] D. Lee, S.A. Long, J.L. Adams, G. Chan, K.S. Vaidya, T.A. Francis, K. Kikly, J.D. Winkler, C.-M. Sung, C. Debouck, Potent and selective nonpeptide inhibitors of caspases 3 and 7 inhibit apoptosis and maintain cell functionality, J. Biol. Chem. 275 (2000) 16007–16014.